BIOCHEMISTRY
including biophysical chemistry & molecular biology

Article

pubs.acs.org/biochemistry

Structural Analysis of a Protective Epitope of the *Francisella tularensis* *O*-Polysaccharide

Michael J. Rynkiewicz,[†] Zhaohua Lu,[‡] Julia H. Hui,[‡] Jacqueline Sharon,[‡] and Barbara A. Seaton*[,†]

[†]Department of Physiology and Biophysics and [‡]Department of Pathology and Laboratory Medicine, Boston University School of Medicine, Boston, Massachusetts 02118, United States

ABSTRACT: *Francisella tularensis* (Ft), the Gram-negative facultative intracellular bacterium that causes tularemia, is considered a biothreat because of its high infectivity and the high mortality rate of respiratory disease. The Ft lipopolysaccharide (Ft LPS) is thought to be a main protective antigen in mice and humans, and we have previously demonstrated the protective effect of the Ft LPS-specific monoclonal antibody Ab52 in a mouse model of respiratory tularemia. Immunochemical characterization has shown that the epitope recognized by Ab52 is contained within two internal repeat units of the *O*-polysaccharide [O-antigen (OAg)] of Ft LPS. To further localize the Ab52 epitope and understand the molecular interactions between the antibody and the saccharide, we determined the X-ray crystal structure of the Fab fragment of Ab52 and derived an antibody−antigen complex using molecular docking. The docked complex, refined through energy minimization, reveals an antigen binding site in the shape of a large canyon with a central pocket that accommodates a V-shaped epitope consisting of six sugar residues, α-D-Gal*p*NAcAN(1→4)-α-D-Gal*p*NAcAN(1→3)-β-D-Qui*p*NAc(1→2)-β-D-Qui*p*4NFm-(1→4)-α-D-Gal*p*NAcAN(1→4)-α-D-Gal*p*NAcAN. These results inform the development of vaccines and immunotherapeutic/immunoprophylactic antibodies against Ft by suggesting a desired topology for binding of the antibody to internal epitopes of Ft LPS. This is the first report of an X-ray crystal structure of a monoclonal antibody that targets a protective Ft B cell epitope.

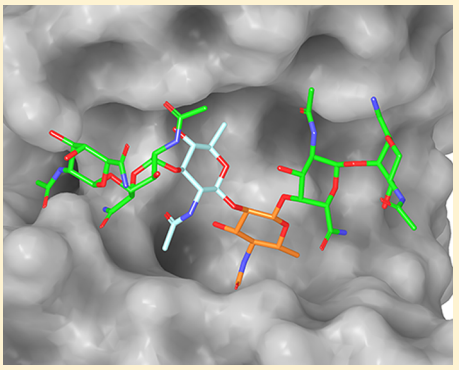

Francisella tularensis (Ft), the Gram-negative intracellular bacterium that causes tularemia, is a category A potential bioterrorism agent, specifically the highly virulent type A subspecies.[1−5] Although tularemia is normally treated with antibiotics, respiratory tularemia, the most severe form of the disease, is still associated with considerable morbidity and up to 2% mortality in treated patients.[1,3−6] This and the threat of engineered antibiotic-resistant Ft variants for bioterrorism make the development of vaccines and immunotherapies for tularemia a priority. An Ft type B live vaccine strain (LVS) is partially protective against Ft in humans but is not currently licensed because of safety concerns.[6,7] A subunit vaccine based on protective Ft epitopes would be an alternative.

Ft lipopolysaccharide (Ft LPS), the main component of the bacterial outer membrane,[8−13] is a major protective antigen in mice[10,14−22] and guinea pigs,[20] and circumstantially in humans.[23] It is comprised of lipid A, a core oligosaccharide, and an *O*-polysaccharide [O-antigen (OAg)] consisting of variable numbers of tetrasaccharide repeats (Figure 1).[8−12,24] We have previously reported that anti-Ft LPS mouse monoclonal antibodies (mAbs) of the IgG2a isotype, the mouse analogue of human IgG1,[25] can confer survival to BALB/c mice infected intranasally with an otherwise lethal dose of LVS.[17,26] We further characterized the Ab52 IgG2a mAb and showed it to be specific for a repeating internal epitope of Ft OAg spanning two tetrasaccharide OAg repeats.[26] Ab52 has the highest avidity for Ft LPS among three anti-LPS IgG2a mAbs that bind to repeating internal OAg epitopes.[27] In vivo efficacy studies showed Ab52 prolongs survival of BALB/c mice infected intranasally with the highly virulent type A strain SchuS4 in addition to conferring survival on mice infected intranasally with LVS.[26]

To further localize the Ab52 epitope within the two-repeat span of Ft OAg and understand the binding specificity and basis for recognition between the antibody and the saccharide, we determined the X-ray crystal structure of the Fab fragment of Ab52 and derived an antibody−antigen complex using molecular docking. The docked complex shows a V-shaped epitope encompassing six of the eight sugar residues, with the central disaccharide, at the point of the V, buried in a pocket deep inside the center of the floor of a large canyon-shaped Ab52 binding site. Analysis of the antigen binding site shows that other possible modes of binding of the Ft OAg are not compatible with the antibody topology.

EXPERIMENTAL PROCEDURES

Deduced Amino Acid Sequence Determination. The amino acid sequences of the heavy (H) and light (L) chain variable (V) regions of Ab52 were deduced from the nucleotide sequences following reverse transcription−polymerase chain reaction (RT−PCR) amplification of the respective mRNAs

Received: November 14, 2011
Revised: June 18, 2012
Published: July 2, 2012

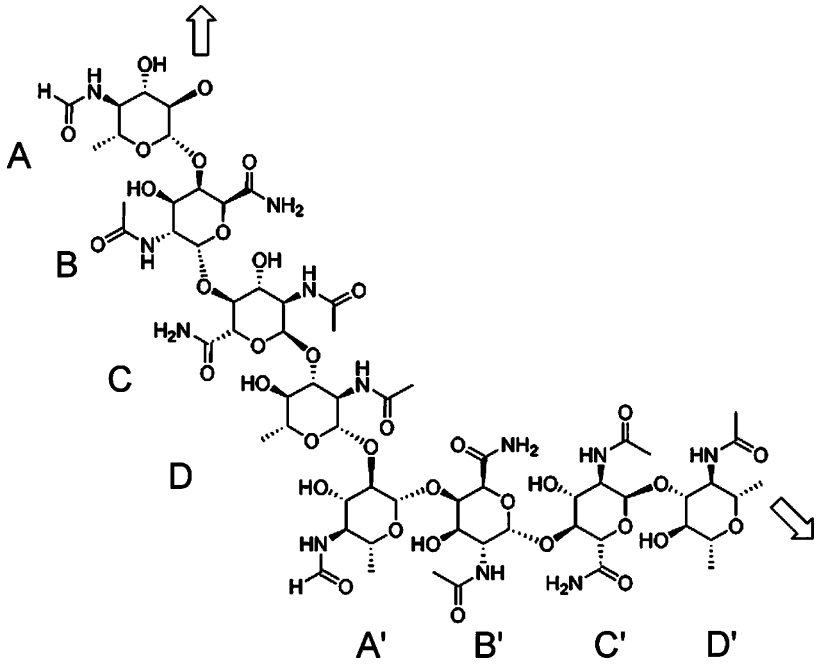

Figure 1. Tetrasaccharide repeat of Ft OAg, consisting of the indicated sugars 2)-β-D-Qui*p*4NFm(1→4)-α-D-Gal*p*NAcAN(1→4)-α-D-Gal*p*NAcAN(1→3)-β-D-Qui*p*NAc(1→, designated ABCD. Two repeats are shown, with the sugars in the second repeat distinguished by a prime. Arrows indicate additional repeats on either side of the octasaccharide.

from cultured Ab52 hybridoma cells as previously described.[28] For the H chain, three PCRs were performed, using reverse primer CH1-γ-LS and forward primer VH1, VH2, or VH3. For the L chain, two PCRs were performed, using reverse primer CL-κ-LS, and forward primer VL1 or VL2. PCR products were visualized by agarose gel electrophoresis, and the V primer yielding the best cDNA amplification (for each VH and VL) was considered the closest match to the actual hybridoma-derived V region gene sequence. These primers were VH2 (GAG GTG CAG CTT CTC GAG TCT GGG GCT GAG CTT GTG AGG CTT GG, spanning the first 15 VH codons) and VL1 (GAG CTC GTG ATG ACA CAG ACT CCA TCC TCC CTG CCT G, which spans the first 12 VL codons). The selected PCR products were gel purified and cloned into plasmid vector pCR 2.1-TOPO (Invitrogen, Carlsbad, CA) following the manufacturer's instructions, and plasmids containing PCR products were subjected to nucleotide sequencing at the Dana-Farber/Harvard Cancer Center DNA Resource Core (Boston, MA) using the T7 primer.

Homology to immunoglobulin (Ig) germline genes was assessed by IgBlast (http://www.ncbi.nlm.nih.gov/igblast/), and the nucleotide sequences imposed by the forward primers were replaced with those of the homologous germline genes [VH-J558.f (97.1% identical nucleotides) and Vκ-8−24 (99.0% identical nucleotides)]. Conversion to amino acid sequences was achieved with EMBOSS Transeq (http://www.ebi.ac.uk/Tools/emboss/transeq/index.html), and the positions of complementarity-determining regions (CDRs) were determined as suggested by North et al.[29]

Preparation of Ab52 Fab for Crystallization. Ab52 Fab was prepared for crystallization from purified IgG2a using the Pierce Fab Preparation Kit (Thermo, Rockford, IL). For crystallization trials, the Fab was concentrated to 33 mg/mL, as determined by absorbance at 280 nm, using a YM-10 Centricon Centrifugal Filter Device (Millipore, Bedford, MA).

Crystal Structure Determination. Crystals of Ab52 Fab were grown in hanging drops in Linbro plates by mixing 1 μL of Fab [33 mg/mL in 20 mM Tris buffer (pH 7.5), 150 mM NaCl, and 0.02% NaN_3] with 1 μL of reservoir solution [0.1 M Tris buffer (pH 7.5) and 24% (w/v) PEG 8000] and equilibrating over 0.5 mL of reservoir solution in a sealed well at 17 °C. Crystals grew within a few days. Prior to being frozen in a nitrogen stream at −180 °C, the crystal was soaked in reservoir solution with 20% (v/v) glycerol added as a cryoprotectant. Diffraction data were collected on an RAXIS-IV imaging plate detector mounted on a Rigaku RU-300 rotating anode generator. Data indexing, integration, and merging were performed with DENZO and SCALEPACK.[30] The crystal belongs to space group $P2_1$, with the following unit cell dimensions: a = 35.953 Å, b = 131.491 Å, c = 86.805 Å, and β = 96.872°.

The structure was determined using molecular replacement as implemented in the AutoMR function of Phenix,[31] using as search models the L chain of anti-ApcT transporter antibody 7F11 [Protein Data Bank (PDB) entry 3GI8[32]] and the H chain of anti-OspB-CT bactericidal Fab-H6831 (PDB entry 1RJL[33]) less the coordinates for the third H chain complementarity-determining region (CDRH3) loop. Inspection of initial maps showed interpretable electron density fitting two Fab molecules in the asymmetric unit. The Ab52 sequence determined above was introduced into the structure using Phenix AutoBuild. Iterative cycles of manual rebuilding and refinement were then undertaken with Coot[34] and Phenix until all interpretable electron density was modeled. For the first 15 residues of the H chain and the first 12 residues of the L chain, the sequence was modified to the germline sequence, which fit the electron density better than the PCR primer sequences used for sequencing. It was noted that in many antibody structures, an N-terminal Gln or Glu residue is observed in a cyclized form as pyroglutamic acid.[35] However, refinement of the Ab52 H chain N-terminal Gln as pyroglutamate resulted in

dx.doi.org/10.1021/bi201711m | *Biochemistry* 2012, 51, 5684−5694

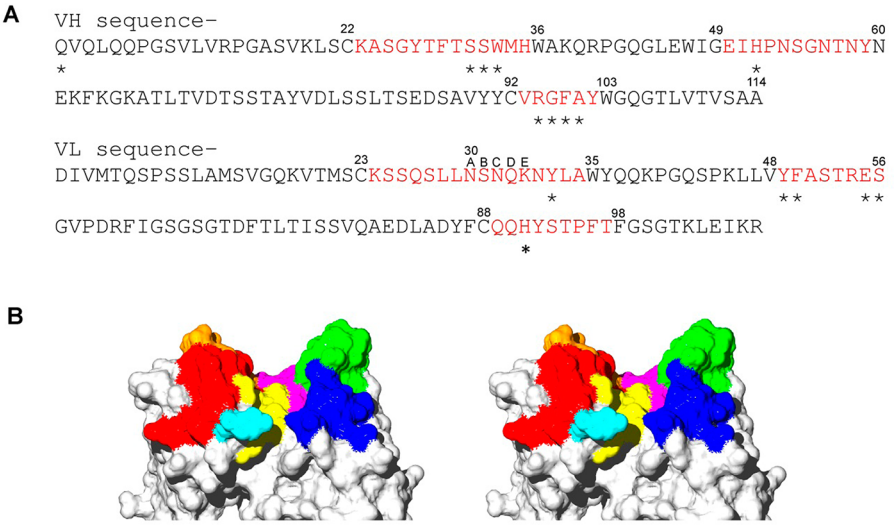

Figure 2. V region deduced amino acid sequence and crystal structure of Ab52 Fab. (A) Deduced amino acid sequences for Ab52 VH and VL. The CDRs, as defined by North et al.,[29] are colored red. The residue numbers at the ends of the CDRs are indicated. There are five residues in CDRL1 following residue 30 that are labeled as residues 30A–30E, following Kabat numbering as modified by Al-Lazikani et al.[63] Residues with an asterisk below them are implicated in antigen recognition by the docking studies. (B) Wall-eyed stereo diagram of the molecular surface of Ab52 Fab showing a side view of the antigen binding site. The surface-contributing areas from the CDRs are colored red (CDRH1), orange (CDRH2), yellow (CDRH3), green (CDRL1), blue (CDRL2), and purple (CDRL3). Residue H-Q1 is also colored cyan.

higher *R* factors. Therefore, the final model contains glutamine as the first H chain residue.

For crystal soaking experiments, a purified fraction of a 2-OAg repeat Ft oligosaccharide (84% pure as estimated from mass spectrometry data, with contaminating three-, four-, and five-repeat oligosaccharides as well as a core-attached single-repeat oligosaccharide), obtained from Q. Wang, C. Costello, and J. Zaia,[24,26] was dissolved in the crystal mother liquor to a concentration of approximately 0.5 mM. A crystal of Ab52 Fab was then soaked in this solution for 2 h, and X-ray data were collected. The structure was determined by difference Fourier using the unliganded coordinates as a starting model; however, no electron density for the ligand was observed. Soaking for longer periods in the same solution destroyed the crystal diffraction.

Molecular Docking. For docking, removal of solvent atoms, addition of hydrogens, hydrogen bond network optimization, and assignment of charges to the crystal structure coordinates were conducted using the Protein Preparation Wizard as implemented in Maestro.[36] Four grids for docking were then calculated with Glide[37−40] using default values. For Ab52 dockings, the centers of the grids were located at a point in the putative antigen binding site close to the side chain of H chain Glu50, where a Tris molecule was located in electron density maps, or at a point close to the side chains of L chain His91, covering the other side of the antigen binding site cleft. Grids were also calculated for each Fab present in the asymmetric unit of the crystal structure after superposition of the two Fabs, bringing the total to four grids.

Starting coordinates of the repeat unit of Ft OAg[8] or sugar monosaccharides were built using the tools in Maestro. Methyl groups were added to positions where the full-length Ft OAg chain would be extended to mimic the missing glycosidic bonds rather than leaving these positions as free hydroxyl groups. A mixed Monte Carlo torsion/low-mode sampling conformational search then was performed in Macromodel[41] using a modified OPLS-2005 force field. Redundant conformations were eliminated using a 1.0 Å all-atom root-mean-square deviation (rmsd) cutoff, and the extended sampling option was used. Each of the resulting starting conformations was then docked into the calculated grids using Glide and the OPLS-2005 force field. For the Glide runs, default parameters in Standard Precision mode were used except that 50000 poses were kept for the initial phase of docking, the scoring window was increased to 200, the expanded sampling mode was used, the best 1000 poses were kept for energy minimization, the maximal number of minimization steps was set to 500, and up to 10 poses were selected for postdocking minimization and output. After docking, the poses from the two Fabs centered on the same point were combined and clustered with XCluster using all atoms in the rmsd calculation. The clustering level was set at a value such that the threshold distance was ~2.0 Å.

Model of the Complex of Ft OAg with Ab52. A calculated version of the Ft OAg was modeled using Maestro. Carbohydrates are flexible molecules but have favored values of their glycosidic bond torsion angles that make a good starting point for modeling purposes.[42] First, a conformational map for each glycosidic bond in the Ft OAg was created to determine the most favored values of glycosidic bonds φ (defined as the H1−C1−Ox−Cx torsion angle) and ψ (defined as the C1−Ox−Cx−Hx torsion angle) for the Ft OAg. Multiple starting models were used for each glycosidic bond, as this allows for better sampling of the effects of the sugar side chains on the glycosidic bond under consideration. In this case, the tetrasaccharide models used in the docking calculations were used as starting models for the conformational maps. Only the middle glycosidic bond of each tetrasaccharide was tested to allow long-range interactions from distal saccharides to be considered. The φ and ψ angles of these middle glycosidic bonds were then set to values between 0° and 360° in 20° increments and minimized in an OPLS-2005 force field using Macromodel. The map was then made by plotting the lowest-energy value obtained from the set of starting OAg models for each point sampled in torsion space. The global lowest-energy torsions from the maps were used as starting conformations to build out the entire Ft OAg. Eight OAg repeat units were then

dx.doi.org/10.1021/bi201711m | *Biochemistry* 2012, 51, 5684−5694

minimized in an OPLS-2005 force field in Macromodel to generate the final structure. This model was used to generate the docked conformation of the two-repeat Ft OAg with Ab52 by aligning the docked pose from Glide with the A ring from the Ft OAg structure generated in Macromodel. The seven other sugars were adjusted by torsion to remove poor contacts with the protein. The resulting docked sugar−antibody complex was then minimized in Macromodel in an OPLS-2005 force field to remove any remaining bad contacts. During the calculation, antibody residues within 5 Å of the docked Ft OAg were allowed to move freely, the next shell of residues within 5 Å was restrained with a force constant of 200, and all other atoms were frozen.

RESULTS

Crystallographic Analysis of Ab52. To define the target epitope of Ab52, we determined the crystal structure of the Fab fragment of Ab52, using the deduced VH and VL region amino acid sequences shown in Figure 2A. Ab52 diffraction data were collected to a resolution of 2.1 Å. The crystal structure was determined using molecular replacement and then refined to good geometry and agreement with the diffraction data (Table 1). There are two outliers on the Ramachandran plot, suggesting disfavored backbone conformations. These are the two L chain Ala51 residues. This position is the third residue of the second L chain CDR loop (CDRL2), which is typically in a turn conformation in antibody structures, and the electron density maps show clear density for the backbone atoms.

Table 1. X-ray Crystal Data Collection and Refinement Statistics[a]

Data Collection	
no. of reflections	46183 (4572)
data cutoff	$I \leq -3\sigma$
$I/\sigma(I)$	13.8 (3.9)
completeness (%)	99.4 (99.4)
redundancy	3.0 (2.7)
R_{merge}	0.075 (0.337)
Refinement	
R_{work}	0.186
R_{free}	0.220
no. of atoms	7348
average *B* factor	
protein	20.7
waters	26.8
Tris/glycerol molecules	26.4

[a]The resolution limits overall were 15−2.1 Å; the numbers in parentheses are the values for the highest-resolution shell (2.17−2.1 Å).

The final crystallographic model contains two Fab molecules comprising L chain residues 1−211 and H chain residues 1−127 and 134−213, four glycerols, three Tris molecules, and 820 water molecules. There was no interpretable density for H chain residues 128−133; however, because these are in the constant (C) domain located far from the antigen binding site, the missing residues are unlikely to affect further calculations. The two Fab molecules that comprise the asymmetric unit show slight structural differences resulting from a 5° difference in the elbow angle formed between the V and C domains of the two chains. The angles were 133° and 138°, calculated using RBOW.[43] This variation is likely due to crystal packing and suggests some flexibility in the Fab. However, the V domains (H chain amino acids 1−114 and L chain amino acids 1−108) overlay well with an rmsd of 0.60 Å calculated using α-carbons, suggesting little effect of crystal packing on the antigen binding site.

Although glycerol is often found in the binding sites of carbohydrate binding proteins, none of the four bound glycerol molecules are in the antigen binding sites of either of two Fab molecules in the asymmetric unit. One glycerol molecule binds to the H chain constant domain where it interacts with H-Q156 and H-V159. Three other glycerol molecules are located in the variable domains underneath the antigen binding sites. One of these glycerols is in a pocket formed by residues H-Q39, H-G44, H-L45, L-Q38, L-F87, and L-G99. The other two are in a site common to both Fab molecules, a pocket formed by L-Q37, L-K39, L-K45, L-L47, L-P59, L-R61, L-F62, L-E81, and L-D82.

One Tris molecule is found in the antigen binding site of each Fab molecule in the asymmetric unit, where they similarly interact with H-W33, H-H35, and H-E50, making hydrogen bonds to these side chains. The third Tris molecule is bound on the outside portion of the CDRL1 and CDRL2 loops where it interacts with residues L-K30F, L-N31, L-F50, L-A51, L-S52, and L-G66.

Ab52 has a canyon-type antigen binding site,[44] with open ends and steep sides, which can accommodate a large antigen like the repeating unit of the Ft OAg (Figure 2B). One wall of the canyon is formed by CDRH1 and CDRH2 as well as the N-terminal Gln residue; the other wall is formed by residues in CDRL1 and CDRL2, and the floor of the canyon is formed by residues from CDRH3 and CDRL3 (Figure 2B). The binding site has several charged residues in the walls of the canyon; in addition to the aforementioned H-E50, there are H-H35, H-R94, and L-E55. A fifth charged residue, L-H91, is located in the floor of the canyon. The remaining residues of the binding site are primarily hydrophobic on the floor of the canyon, with polar residues predominating on the walls of the canyon.

All of the CDR loops, with the exception of CDRH3, fall into conformational clusters.[29] CDRL1, CDRL2, CDRL3, CDRH1, and CDRH2 are in conformations L1-16-1, L2-8-1, L3-9-*cis*7-1, H1-13-1, and H2-10-1, respectively. The CDRH3 loop is only six residues long, comprising the sequence ^{93}VRGFAY^{98}, which precludes categorizing the loop by its anchor region. A search on Abysis (http://www.bioinf.org.uk/abysis/index.html) revealed eight antibody structures with six-residue CDRH3 loops (Table 2), and superimposition of these loops (Figure 3) suggests CDRH3 loops of this size may fold similarly in the cases found to date. However, there appear to be no consensus sequence signatures for the loop, other than the length, despite the good fit of the loops to one another. Analysis of the backbone conformations of the superimposed CDRH3 loops reveals the structural similarities between the loops. The first two residues of the loop are invariably in a β-sheet conformation. Most of the third residues are in the left-handed helix or glycine region of the Ramachandran plot making the turn, with the exception of the less well fit loops from Table 2, which are either β-sheet (PDB entries 2DDQ and 3GGW) or α-helical (PDB entries 1NSN and 1EMT) conformations. The fourth and fifth residues of the loop adopt α-helical conformations, with five amino acid exceptions from PDB entries 1NSN, 2DTG, 1EMT, and 2R4R. The last residue is in a β-sheet conformation, with one exception (PDB entry 1NSN). Therefore, with the exception of PDB entry 1NSN,

dx.doi.org/10.1021/bi201711m | *Biochemistry* 2012, 51, 5684−5694

Table 2. Comparison of Structural Similarity between Ab52 and Published Antibody Structures with CDRH3 Loops of Six Residues

antibody	antigen specificity	PDB entry	sequence	rmsd[a]
Ab52	Ft OAg	3UJT	VRGFAY	0.10
N10	staphylococcal nuclease	1NSN[56]	TRGNGD	1.59
VRQ14	prion protein	1TQB[57]	TRGTDY	0.28
LA2	outer surface protein A	1FJ1[58]	ARGLDS	0.73
83-14	insulin receptor	2DTG[59]	AREWAY	0.75
no name	fullerene	1EMT[60]	ATSSAY	1.58
no name	β2 adrenoceptor	2R4R[61]	VRGFGY	0.83
R310	(*R*)-4-hydroxy-2-nonenal histidine	2DDQ[62]	APYGGY	1.19
F22-4	*S. flexneri* OAg	3GGW[52]	FLPMDY	0.97

[a]The rmsd was calculated using backbone atoms from the CDRH3 loop residues when fit to CDRH3 of the Ab52 structure. For Ab52, the rmsd value was the fit between the two Fab H chains present in the structure. In cases where more than one structure was determined for an antibody, the structure with the best resolution and refinement statistics was aligned. In cases where more than one antibody chain was present in the structure, including Ab52, the first H chain was used in the calculation.

Figure 3. Overlay of six-residue CDRH3 loops. The CDRH3 loops from the structures listed in Table 2 are shown as α-carbon traces. The loops were superimposed onto the H chain of the Ab52 Fab structure using Iterative Magic Fit in Deepview. The loops are colored blue and light blue for Ab52, red for Ab N10, orange for Ab VRQ14, yellow for Ab LA2, green for Ab 83-14, cyan for the anti-fullerene Ab, purple for the anti-β2 adrenoceptor Ab, magenta for Ab R310, and gray for Ab F22-4.

the secondary structural elements among all six-residue CDRH3 loops determined to date share a common fold. Interestingly, the F22-4 antibody, which has a six-residue CDRH3 that contains a *cis*-proline, also recognizes an OAg (from *Shigella flexneri* serotype 2a), although it is branched, unlike the linear Ft OAg recognized by Ab52.

Molecular Docking and Modeling of the Antibody–Antigen Complex. Attempts to soak a 2-OAg repeat Ft oligosaccharide into Ab52 Fab crystals were unsuccessful; therefore, mapping of specific interactions between Ab52 and the Ft OAg was pursued using molecular docking techniques. For docking calculations, two grids were made because a single grid in Glide[37−40] would not encompass the entire antigen binding site. The first grid was centered on the ordered Tris molecule found in the putative antigen binding site, because it is possible that the Tris molecule, having multiple hydroxyl groups, acts as a mimic of one of the Ft OAg sugars. There were no solvent molecules other than waters observed in the antigen binding site to further guide positioning of the grids; therefore, the second grid was positioned to encompass the remainder of the putative antigen binding site.

The repeat unit of the Ft OAg is four sugar residues long, and previous data indicated that Ab52 binds to an internal site that spans two OAg repeats.[26] Therefore, a strategy was employed in the docking calculations that would allow sampling of the length of the OAg by modeling the four possible tetrasaccharides available to the antibody on the OAg. These models consisted of sugars ABCD, BCDA′, CDA′B′, and DA′B′C′ (Figure 1). After docking, the top scoring clusters were analyzed to eliminate poses where the ends of the tetrasaccharide were buried, because these structures cannot be extended into the full-length OAg. Thus, a single, top-scoring cluster of structures for each docked tetrasaccharide was obtained (Table 3). The Glide scores for the docked

Table 3. Glide Results of Dockings with Tetra- and Monosaccharides to Ab52

saccharide	Glide score[a]
ABCD	−8.0
BCDA′	−8.5
CDA′B′	−7.7
DA′B′C′	−7.9
1,2-O-Me-β-Qui4NFm	−5.8
1,2-O-Me-β-Qui	−5.2
1,2-O-Me-β-Glc4NFm	−5.3

[a]The Glide score is equal to 0.05 × vdW + 0.15 × Coul + Lipo + HBond + Metal + Rewards + RotatableBonds + Site (vdW, van der Waals energy; Coul, Coulomb energy; Lipo, lipophilic term; Hbond, H-bonding term; Metal, metal binding term; Rewards, rewards and penalties; RotatableBonds, penalty for freezing rotatable bonds; Site, polar interactions in the active site). Detailed descriptions of these parameters are given in ref 37. The units are kilocalories per mole.

tetrasaccharides were in the range of −7.7 to −8.5, considered very good using standard precision mode for ligands binding to proteins with binding sites of comparable depth (http://www.schrodinger.com/kb/639).

The four docked tetrasaccharide structures in Table 3 were analyzed to select the best prediction of the OAg–antibody complex. In an ideal docking case, the tetrasaccharides should overlay with one another to form a single, continuous Ft OAg model, sliding one saccharide down or up the chain with each model. For example, comparison of the best ABCD and BCDA′ docked structures ideally would show exact overlay of rings B–D. Therefore, each of the best scoring structures from the docking was inspected to see if there was significant overlap between that pose and all the output docking structures from tetrasaccharides that were translocated one sugar residue toward both the reducing and nonreducing ends of the putative Ft OAg. The only structure in which extension in both directions was found was the CDA′B′ docked structure, which showed significant overlap with the BCDA′ and DA′B′C′ docked structures, with rmsd values of 3.3 and 2.3 Å, respectively, calculated using all atoms from the three common sugars from each structure set (Figure 4). The overlay is very good near the centers of the structures and more variable toward the ends. Because the end sugars in the models are not bound to the next sugar in the putative Ft OAg chain, they may have more conformational flexibility in their glycosidic bonds and may access conformations forbidden to the same sugars in the full-length Ft OAg. Therefore, the end sugars may be in

dx.doi.org/10.1021/bi201711m | *Biochemistry* 2012, 51, 5684−5694

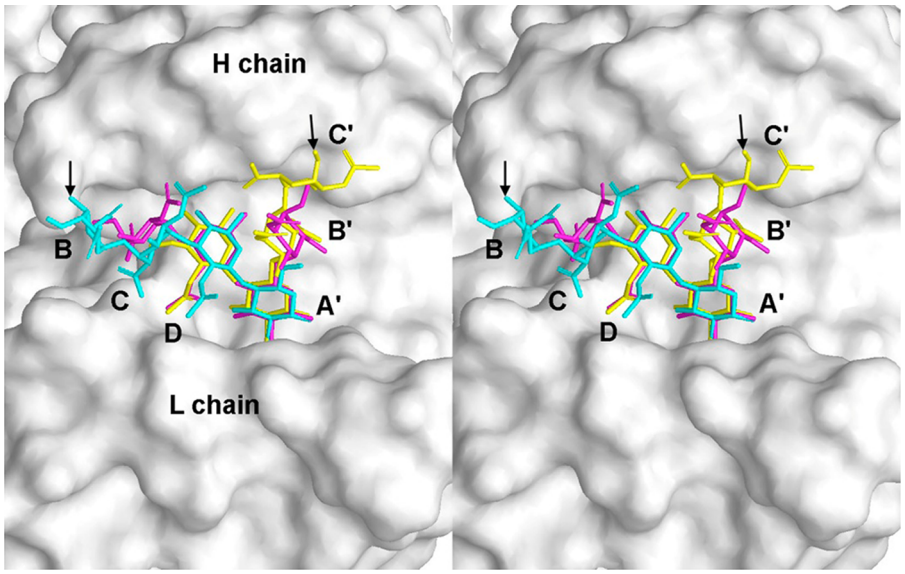

Figure 4. Wall-eyed stereo diagram showing tetrasaccharides docked to Ab52 Fab. Shown are the docked poses from Glide of tetrasaccharides BCDA′ (aqua), CDA′B′ (magenta), and DA′B′C′ (yellow). The antibody is rendered as a gray molecular surface, oriented looking down into the antigen binding site with the H chain on top. The remainder of the Ft OAg chain would extend in both directions at the positions indicated by the arrows.

Table 4. Glycosidic Bond Angles (φ, ψ) of Docked Ft OAg Tetrasaccharides and the Final Octasaccharide Model

glycosidic bond	ideal	BCDA′	CDA′B′	DA′B′C′	ABCDA′B′C′D′
Qui4NFm(A)−GalNAcAN(B)	20°, −40°				31°, −7°
GalNAcAN(B)−GalNAcAN(C)	−40°, 0°	−42°, −23°			−46°, 0°
GalNAcAN(C)−QuiNAc(D)	−40°, 0°	−53°, −41°	−66°, −65°		−40°, −42°
QuiNAc(D)−Qui4NFm(A′)	60°, 40°	55°, 12°	50°, −5°	48°, 7°	50°, 28°
Qui4NFm(A′)−GalNAcAN(B′)	20°, −40°		58°, 21°	55°, 30°	27°, −42°
GalNAcAN(B′)−GalNAcAN(C′)	−40°, 0°			−41°, −8°	−42°, −4°
GalNAcAN(C′)−QuiNAc(D′)	−40°, 0°				−32°, −25°

spurious conformations in the docking that create contacts with the protein that are not biologically relevant but contribute favorably to the docking score. The presence of biologically irrelevant conformations may also explain why the BCDA′ and DA′B′C′ structures did not score at the top of the docking output, because these spurious conformations will score higher in the docking algorithm.

The tetrasaccharides dock in conformations that show good glycosidic bond values (Table 4), with the exception of the A′B′ glycosidic bonds, which have torsion energies more than 5 kcal/mol higher than the global minimum. It should be noted that unfavored glycosidic angles are observed in crystal structures found in the GlycoMaps[41] database, which is organized by sugar and linkage. For example, the 1→4 glycosidic linkage in maltose has unfavorable geometry in 5.3% or 96 of 1822 structures in the Protein Data Bank (http://www.pdb.org). As there are no examples of the present sugars in the GlycoMaps database, no direct comparison can be made with similar glycosidic bonds in crystal structures. In our model, the unfavorable glycosidic bond conformation appears to be an artifact of the Glide scoring function. The torsion angle of the bond is unfavorable (φ = 58°, and ψ = 21°) because the C4 hydrogen of the B′ ring eclipses C1 of the A′ ring. However, this rotamer allows the B′ ring to pack against the D ring, giving this pose fewer solvent-exposed atoms, and thus a better Glide score even at the expense of good geometry. There is a very similar pose in the docking output (rmsd of 1.5 Å calculated with all atoms) that does not score as well (Glide score = −6.9) but has favorable glycosidic bond angles (φ = 47°, and ψ = 13°), lending credence to this idea.

Docking with monosaccharides from Ft OAg was undertaken to determine whether they would converge to binding sites similar to those observed for the tetrasaccharides. Docking of the A ring monosaccharide from Ft OAg converged to a similar binding pocket as the A′ ring in the tetrasaccharide dockings (rmsd of 3.4 Å calculated using all atoms). This pocket, deep in the floor of the antibody canyon, is formed by the CDRL2, CDRL3, and CDRH3 loops, specifically residues L-Y49, L-F50, L-H91, and H-F96. Docking with the B, C, and D sugars also converged to the same pocket as A; however, these poses were incompatible with the tetrasaccharide structure. Docking of a quinovose sugar lacking the 4-*N*-formyl modification resulted in an altered pose and reduced the estimated binding energy, suggesting that this group is critical for recognition of the A sugar. Interestingly, a glucose analogue of the A sugar (1,2-O-Me-β-Glc4NFm), which has a hydroxyl group on the 6-carbon of the sugar, docked in a pose identical to that of the A sugar and with a similar energy score despite the extra OH group.

To evaluate whether the binding mode determined by docking of tetrasaccharides to Ab52 would be compatible with longer OAg fragments that are present on the surface of Ft, a two-repeat model of Ft OAg complexed with Ab52 Fab was created by overlay of the C, D, and A′ sugars of the docked CDA′B′ tetrasaccharide structure and the model of the Ft OAg

dx.doi.org/10.1021/bi201711m | *Biochemistry* 2012, 51, 5684−5694

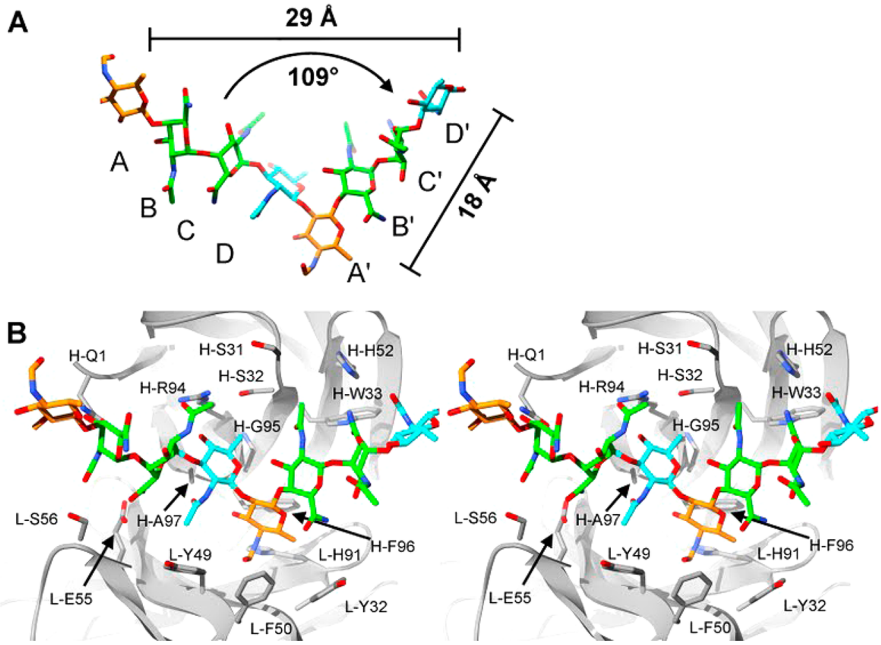

Figure 5. Docked model of Ft OAg bound to Ab52. (A) Calculated model of the Ft OAg built as outlined in Experimental Procedures. The sugar rings are colored by type, with orange carbons for Qui4NFm residues (A), green carbons for GalNAcAN residues (B and C), and cyan carbons for QuiNAc residues (D). Two repeat units (eight sugars) are shown. (B) Wall-eyed stereo diagram of the interactions between the Ft OAg and the antibody in the final docked model of the Ft OAg–antibody complex. The Ft OAg sugars are colored as in the top panel, and the carbons for protein atoms are colored gray.

calculated from the conformational search (Figure 5). In the calculated model, each repeat unit is in a linear conformation, ~18 Å in length. However, the β1→2 connection between the D and A′ rings makes a kink in the sugar chain such that two repeats form a V shape with the A ring at the point of the V and the arms make a 109° angle (Figure 5A). After superimposition of the calculated model of Ft OAg onto the C, D, and A′ sugars of the docked tetrasaccharides and energy minimization, a two-repeat unit model of Ft OAg in the Ab52 antigen binding site was generated. The glycosidic bonds of the sugars in this final docked model of the Ft OAg–antibody complex were in favorable conformations (Table 4) with no bad contacts. Analysis of the docked Ft OAg structure in the antigen binding site shows that the epitope being recognized by Ab52 spans two repeat units, with the majority of the interaction coming from the central D and A′ sugars (Figure 5B and Table 5). Starting from the nonreducing end of the OAg chain, the B ring docks between Gln1 of the H chain (H-Q1) and Ser56 of the L chain (L-S56), making hydrogen bonds to the side chains through the O3 and *N*-acetyl carbonyl carbon group (Figure 5B). The C sugar interacts more extensively with the antibody in the model, making a hydrogen bond to the side chain of L-E55 through its 6-amide group and another to the side chain of H-R94 through its *N*-acetyl group.

Table 5. Summary of Saccharide Contacts from the Docked Structures to Ab52

property	A	B	C	D	A′	B′	C′	D′
total no. of contacts	0	6	7	17	19	7	4	1
no. of hydrogen bonds	0	3	2	0	1	0	1	0
buried surface area (Å^2)	0	21	12	70	96	26	7	0

The D and A′ sugars make the most extensive interactions with the antibody. The D sugar is bound between the walls of the canyon, making key hydrophobic interactions. The hydrophobic face of the sugar ring is interacting with the side chain of H-A97. The methyl group of the *N*-acetyl group is interacting with the side chain of L-Y49. The C6 methyl group of the sugar is bound in a side pocket formed by the carbon atoms of the H-R94 side chain, H-G95, and H-S32.

The A′ sugar is anchored by interactions between the *N*-formyl group and a small pocket on the antibody formed by the side chains of L-Y49, L-F50, L-H91, and H-F96, where it makes a hydrogen bond to the L-H91 side chain. The only other functional groups on the Ft OAg similar to the *N*-formyl group are *N*-acetyl, whose methyl group would be too large to fit in this pocket and would have to adopt an unfavorable *cis* conformation, and the amide group of the B sugar, which would place the sugar ring in conflict with several protein residues. Therefore, this pocket appears to be specific for the *N*-formyl group of the A′ sugar. The 6-carbon of the A′ sugar binds in a subsite formed by L-H91, H-F96, and L-Y32.

The last two sugars to contact the antibody in the model are B′ and C′. The B′ sugar interacts with H-S31, H-S32, and H-W33 through its *N*-acetyl group. The C′ sugar makes a hydrogen bond through its amide group to the side chain of H-W33. There is also a potential for the amide group to make a hydrogen bond to the side chain of H-H52, but this requires the His side chain to be unprotonated, which was not the case during the docking calculations. Thus, the model shows six sugars comprising the sequence α-D-Gal*p*NAcAN(1→4)-α-D-Gal*p*NAcAN(1→3)-β-D-Qui*p*NAc(1→2)-β-D-Qui*p*4NFm(1→4)-α-D-Gal*p*NAcAN(1→4)-α-D-Gal*p*NAcAN (BCDA′B′C′) interacting with the antibody using primarily residues from each of the six CDR loops (Figure 2A), as would be expected for an antibody–antigen complex.

dx.doi.org/10.1021/bi201711m | *Biochemistry* 2012, 51, 5684–5694

DISCUSSION

The final docked model of the Ft OAg−antibody complex shows the Ft OAg fitting into a canyon-type[44] antigen binding site on the antibody, where there are contacts to the antibody by six central sugar residues [α-D-Gal*p*NAcAN(1→4)-α-D-Gal*p*NAcAN(1→3)-β-D-Qui*p*NAc(1→2)-β-D-Qui*p*4NFm-(1→4)-α-D-Gal*p*NAcAN(1→4)-α-D-Gal*p*NAcAN (BCDA′B′C′)]. Previous studies had predicted that carbohydrate−antibody complexes would consist of no more than seven saccharides,[45] because of the size limit of a VH−VL pair, and this model conforms to that prediction. Additionally, it was predicted that antibodies recognizing reducing or nonreducing end sites on saccharide chains would have cave or crater-type combining sites, whereas internal sites would be bound by canyon or valley-type combining sites.[46] Consistent with this idea, the antigen binding site of Ab52 Fab is a canyon-type site, with open ends and steep walls.

The interactions between the antibody and the Ft OAg were determined using molecular docking techniques. Soaking of Fab crystals with a two-repeat OAg oligosaccharide was unsuccessful in producing a structure of the Ab−OAg complex, possibly because of a lack of antigen binding site accessibility in the crystal. The crystal contacts do not affect the ligand binding site directly, however, so are unlikely to affect further calculations. In the absence of crystal structure information about the complex, a good prediction of the binding of an antigen to an antibody can be made using molecular docking approaches as implemented in programs such as Glide.[47] A recent benchmark study showed the robustness of Glide, testing its ability to reproduce the crystal structure of 11 antibody−carbohydrate complexes.[47] This study included a variety of antigen binding site structures (six crater, three canyon, and two valley) and carbohydrates varying in length from two to four saccharides. Glide was able to reproduce the crystal structure in all but one case, with an average rmsd for all cases of 1.43 Å between the docked structure and the crystal structure, with most values being <1 Å. These results were obtained in the absence of explicit waters, so the lack of water molecules in the calculation did not adversely affect the results. The ability of Glide to accurately predict carbohydrate−antibody interactions was thus demonstrated.

The model shows that the antibody makes contacts with six sugars, BCDA′B′C′, spanning two repeat units of Ft OAg. The D and A′ sugars are buried the most in the docked complexes. The Ft OAg in both the calculated model and the final docked model of the Ft OAg−antibody complex shows that the A sugars protrude from the linear axis of the polysaccharide chain (Figure 5). Taken together, it is not surprising that the D and A sugars are targeted by the immune system, because they represent an exposed surface unique to Ft OAg.

There is a wealth of immunochemical data available for Ab52,[26,27] and the calculated model is consistent with these observations. Ab52 was found to bind to a ladder of Ft LPS on a Western blot but to bind poorly to the shortest fragments on the blot, unlike the Ft OAg nonreducing end-binding mAb FB11.[27] Competition assays with Ft LPS oligosaccharides with a defined OAg repeat length showed that the Ab52 epitope spans two repeat units, as suggested by the higher potency of the $[ABCD]_2$ core compared to that of the [ABCD] core at competing with Ft OAg for Ab52 binding, and the equal potency of the $[ABCD]_2$ core and the $[ABCD]_3$ core.[26] According to the final docked model of the Ft OAg−antibody complex, $[ABCD]_2$ would make all the potential interactions with the antibody. [ABCD], on the other hand, would occupy only half of the combining site formed by sugars B−D or by sugars A′−C′ in the model and thus would be predicted to have a lower affinity than $[ABCD]_2$. The model also indicates the epitope to be six sugars rather than eight and excludes the sugars at each end of the epitope. These sugars were not observed to make contacts with the antibody in the models.

The docking calculations predict that the Ft OAg binds with a V-shaped epitope buried in a pocket deep in the floor of the canyon-shaped antigen binding site. During the docking calculations, the boundaries used to define the antigen site covered the entire binding site, including the floor and walls of the canyon. Thus, the tetrasaccharides were allowed to sample a large number of potential conformations, but the "point down" conformation of the V-shaped Ft OAg was the one that scored the best. Inspection of the antigen binding site in the Ab52 crystal structure shows that other orientations can be ruled out because they are incompatible with the size and shape of the canyon. For example, the repeating nature of the OAg requires that the carbohydrate chain binds in an orientation parallel to the canyon, so that it extends out through the open ends of the binding site. This requirement is satisfied by the orientation of the epitope in the antigen binding site in the docked model.

At least 13 crystal structures of antibody fragment−OAg complexes from three bacterial sources have been published to date. The structure of Se155-4, an antibody active against the *Salmonella* serogroup B OAg, has been determined by both X-ray crystallography and NMR complexed to tri-, hexa-, and dodecasaccharides.[48−51] The repeating unit in *Salmonella* is the branched tetrasaccharide {→3)α-D-Gal*p*(1→2)[α-D-Abe*p*(1→3)]-α-D-Man*p*(1→4)-α-L-Rha*p*(1→} (A[D]BC), where Abe is the sugar abequose. The second bacterial source is *S. flexneri* serotype 2a, where the structure of antibody F22-4 has been determined in a complex with a peptide mimic and penta- and decasaccharides.[52,53] The repeating unit is a branched pentasaccharide {→2)-α-L-Rha*p*(1→2)-α-L-Rha*p*(1→3)[α-D-Glc*p*(1→4)]-α-L-Rha*p*(1→3)-β-D-Glc*p*NAc(1→} (AB[E]CD). Lastly, SYA/J6, active against the linear *S. flexneri* Y OAg that has a four-sugar repeating unit of sequence →2)-α-L-Rha*p*(1→2)-α-L-Rha*p*(1→3)-α-L-Rha*p*(1→3)-β-D-Glc*p*NAc(1→ (ABCD), has been crystallized complexed to a peptide mimic and tri- and pentasaccharide ligands.[54,55] The Ab52 model complex can be compared to the complex of the antibody SYA/J6−pentasaccharide complex, because they both recognize a linear tetrasaccharide OAg. The binding sites of the two antibodies are very different in sequence and structure, because of the longer CDRH3 loop in SYA/J6, but share a canyon topology. Furthermore, the sugar binding modes are somewhat similar. Each is bound in a V-like conformation, where the point of the V (the A sugar of Ft OAg or the C ring of *S. flexneri* Y OAg) sits deep in the antigen binding site on the floor of the canyon, and the arms of the V interact with the sides of the canyon. It will be interesting to ascertain, as more structures of linear OAg−antibody complexes become available, whether this mode of binding is commonly used in recognition of linear OAgs.

In summary, we determined the crystal structure of the Fab of Ab52, an antibody targeting an internal epitope of Ft OAg that has demonstrated potential as a protective epitope against challenge with Ft. From the crystal structure and molecular docking methods, the Ab52 epitope was deduced to consist of a V-shaped hexasaccharide spanning two OAg tetrasaccharide

repeats, with the D and A′ sugars, at the point of the V, buried in a deep central pocket inside a large canyon-shaped Ab52 binding site. These studies inform the development of vaccines and immunotherapeutic/immunoprophylactic antibodies against Ft by suggesting a desired binding topology for binding of the antibody to internal epitopes of Ft LPS. Furthermore, the basis for recognition between the OAg saccharide and a known protective antibody determined here will allow the evaluation of the quality of human antibodies generated in response to new Ft vaccines in future clinical trials.

■ ASSOCIATED CONTENT

Accession Codes

Crystallographic data have been deposited with the Protein Data Bank as entry 3UJT.

■ AUTHOR INFORMATION

Corresponding Author

*Department of Physiology and Biophysics, Boston University School of Medicine, 715 Albany St., Boston, MA 02118. Telephone: (617) 638-5061. Fax: (617) 638-4041. E-mail: seatonba@bu.edu.

Funding

This work was supported by Contract HHSN272200900054C from the National Institutes of Health.

Notes

The authors declare no competing financial interest.

■ ACKNOWLEDGMENTS

We thank Qi Wang, Catherine Costello, and Joseph Zaia for providing purified Ft oligosaccharides for crystal soaking attempts.

■ ABBREVIATIONS

1,2-O-Me-β-Glc4NF, 1,2-*O*-methyl-4-deoxy-4-formamido-D-glucose; 1,2-O-Me-β-Qui, 1,2-*O*-methyl-6-deoxy-D-glucose; 1,2-O-Me-β-Qui4NFm, 1,2-*O*-methyl-4,6-dideoxy-4-formamido-D-glucose; D-Gal*p*NAcAN, 2-acetamido-2-deoxy-D-galacturonamide; D-Glc*p*NAc, *N*-acetyl-D-glucosamine; D-Qui*p*NAc, 2-acetamido-2,6-dideoxy-D-glucose; D-Qui*p*4NFm, 4,6-dideoxy-4-formamido-D-glucose; L-Rhap, 6-deoxy-L-mannose; Ft, *F. tularensis*; LPS, lipopolysaccharide; LVS, live vaccine strain; mAb, monoclonal antibody; OAg, O-antigen; PCR, polymerase chain reaction; PEG, polyethylene glycol; rmsd, root-mean-square deviation; RT−PCR, reverse transcription−polymerase chain reaction.

■ REFERENCES

(1) Thomas, L. D., and Schaffner, W. (2010) Tularemia pneumonia. *Infectious Diseases in the Clinic in North America 24*, 43−55.

(2) McLendon, M. K., Apicella, M. A., and Allen, L. A. (2006) *Francisella tularensis*: Taxonomy, genetics, and immunopathogenesis of a potential agent of biowarfare. *Annu. Rev. Microbiol. 60*, 167−185.

(3) Sjostedt, A. (2007) Tularemia: History, epidemiology, pathogen physiology, and clinical manifestations. *Ann. N.Y. Acad. Sci. 1105*, 1−29.

(4) Tarnvik, A., and Chu, M. C. (2007) New approaches to diagnosis and therapy of tularemia. *Ann. N.Y. Acad. Sci. 1105*, 378−404.

(5) Dennis, D. T., Inglesby, T. V., Henderson, D. A., Bartlett, J. G., Ascher, M. S., Eitzen, E., Fine, A. D., Friedlander, A. M., Hauer, J., Layton, M., Lillibridge, S. R., McDade, J. E., Osterholm, M. T., O'Toole, T., Parker, G., Perl, T. M., Russell, P. K., and Tonat, K. (2001) Tularemia as a biological weapon: Medical and public health management. *JAMA, J. Am. Med. Assoc. 285*, 2763−2773.

(6) Conlan, J. W. (2011) Tularemia vaccines: Recent developments and remaining hurdles. *Future Microbiol. 6*, 391−405.

(7) Oyston, P. C. (2009) *Francisella tularensis* vaccines. *Vaccine 27* (Suppl. 4), D48−D51.

(8) Vinogradov, E. V., Shashkov, A. S., Knirel, Y. A., Kochetkov, N. K., Tochtamysheva, N. V., Averin, S. F., Goncharova, O. V., and Khlebnikov, V. S. (1991) Structure of the O-antigen of *Francisella tularensis* strain 15. *Carbohydr. Res. 214*, 289−297.

(9) Gunn, J. S., and Ernst, R. K. (2007) The structure and function of *Francisella* lipopolysaccharide. *Ann. N.Y. Acad. Sci. 1105*, 202−218.

(10) Conlan, J. W., Shen, H., Webb, A., and Perry, M. B. (2002) Mice vaccinated with the O-antigen of *Francisella tularensis* LVS lipopolysaccharide conjugated to bovine serum albumin develop varying degrees of protective immunity against systemic or aerosol challenge with virulent type A and type B strains of the pathogen. *Vaccine 20*, 3465−3471.

(11) Prior, J. L., Prior, R. G., Hitchen, P. G., Diaper, H., Griffin, K. F., Morris, H. R., Dell, A., and Titball, R. W. (2003) Characterization of the O antigen gene cluster and structural analysis of the O antigen of *Francisella tularensis* subsp. *tularensis*. *J. Med. Microbiol. 52*, 845−851.

(12) Thirumalapura, N. R., Goad, D. W., Mort, A., Morton, R. J., Clarke, J., and Malayer, J. (2005) Structural analysis of the O-antigen of *Francisella tularensis* subspecies *tularensis* strain OSU 10. *J. Med. Microbiol. 54*, 693−695.

(13) Rhinehart-Jones, T. R., Fortier, A. H., and Elkins, K. L. (1994) Transfer of immunity against lethal murine *Francisella* infection by specific antibody depends on host γ interferon and T cells. *Infect. Immun. 62*, 3129−3137.

(14) Fulop, M., Manchee, R., and Titball, R. (1995) Role of lipopolysaccharide and a major outer membrane protein from *Francisella tularensis* in the induction of immunity against tularemia. *Vaccine 13*, 1220−1225.

(15) Fulop, M., Manchee, R., and Titball, R. (1996) Role of two outer membrane antigens in the induction of protective immunity against *Francisella tularensis* strains of different virulence. *FEMS Immunol. Med. Microbiol. 13*, 245−247.

(16) Fulop, M., Mastroeni, P., Green, M., and Titball, R. W. (2001) Role of antibody to lipopolysaccharide in protection against low- and high-virulence strains of *Francisella tularensis*. *Vaccine 19*, 4465−4472.

(17) Lu, Z., Roche, M. I., Hui, J. H., Unal, B., Felgner, P. L., Gulati, S., Madico, G., and Sharon, J. (2007) Generation and characterization of hybridoma antibodies for immunotherapy of tularemia. *Immunol. Lett. 112*, 92−103.

(18) Savitt, A. G., Mena-Taboada, P., Monsalve, G., and Benach, J. L. (2009) *Francisella tularensis* infection-derived monoclonal antibodies provide detection, protection, and therapy. *Clin. Vaccine Immunol. 16*, 414−422.

(19) Sebastian, S., Dillon, S. T., Lynch, J. G., Blalock, L. T., Balon, E., Lee, K. T., Comstock, L. E., Conlan, J. W., Rubin, E. J., Tzianabos, A. O., and Kasper, D. L. (2007) A defined O-antigen polysaccharide mutant of *Francisella tularensis* live vaccine strain has attenuated virulence while retaining its protective capacity. *Infect. Immun. 75*, 2591−2602.

(20) Khlebnikov, V. S., Vetchinin, S. S., Grechko, G. K., Averina, A. A., Golovlev, I. R., Averin, S. F., Zhemchugov, V. E., Konovalov, S. I., Anisimov, G. A., and Afanas'ev, S. S. (1992) [The preventive activity of monoclonal antibodies specific to the lipopolysaccharide of *Francisella tularensis*]. *Zh. Mikrobiol., Epidemiol. Immunobiol.,*, 67−70.

(21) Li, J., Ryder, C., Mandal, M., Ahmed, F., Azadi, P., Snyder, D. S., Pechous, R. D., Zahrt, T., and Inzana, T. J. (2007) Attenuation and protective efficacy of an O-antigen-deficient mutant of *Francisella tularensis* LVS. *Microbiology (Reading, U.K.) 153*, 3141−3153.

(22) Sebastian, S., Pinkham, J. T., Lynch, J. G., Ross, R. A., Reinap, B., Blalock, L. T., Conlan, J. W., and Kasper, D. L. (2009) Cellular and humoral immunity are synergistic in protection against types A and B *Francisella tularensis*. *Vaccine 27*, 597−605.

(23) Drabick, J. J., Narayanan, R. B., Williams, J. C., Leduc, J. W., and Nacy, C. A. (1994) Passive protection of mice against lethal *Francisella tularensis* (live tularemia vaccine strain) infection by the sera of human recipients of the live tularemia vaccine. *Am. J. Med. Sci. 308*, 83−87.
(24) Wang, Q., Shi, X., Leymarie, N., Madico, G., Sharon, J., Costello, C. E., and Zaia, J. (2011) A typical preparation of *Francisella tularensis* O-antigen yields a mixture of three types of saccharides. *Biochemistry 50*, 10941−10950.
(25) Murphy, K., Travers, P., Walport, M., and Janeway, C. (2008) *Janeway's Immunobiology*, Garland Science, New York.
(26) Lu, Z., Madico, G., Roche, M. I., Wang, Q., Hui, J. H., Perkins, H. M., Zaia, J., Costello, C. E., and Sharon, J. (2012) Protective B-cell epitopes of *Francisella tularensis* O-polysaccharide in a mouse model of respiratory tularemia. *Immunology 136*, 352−360.
(27) Roche, M. I., Lu, Z., Hui, J. H., and Sharon, J. (2011) Characterization of monoclonal antibodies to terminal and internal O-antigen epitopes of *Francisella tularensis* lipopolysaccharide. *Hybridoma Hybridomics 30*, 19−28.
(28) Sharon, J., Sompuram, S. R., Yang, C. Y., Williams, B. R., and Sarantopoulos, S. (2002) Construction of polyclonal antibody libraries using phage display. *Methods Mol. Biol. 178*, 101−112.
(29) North, B., Lehmann, A., and Dunbrack, R. L., Jr. (2011) A new clustering of antibody CDR loop conformations. *J. Mol. Biol. 406*, 228−256.
(30) Otwinowski, Z., and Minor, W. (1997) *Methods Enzymol. 276*, 307−326.
(31) Adams, P. D., Afonine, P. V., Bunkoczi, G., Chen, V. B., Davis, I. W., Echols, N., Headd, J. J., Hung, L. W., Kapral, G. J., Grosse-Kunstleve, R. W., McCoy, A. J., Moriarty, N. W., Oeffner, R., Read, R. J., Richardson, D. C., Richardson, J. S., Terwilliger, T. C., and Zwart, P. H. (2010) PHENIX: A comprehensive Python-based system for macromolecular structure solution. *Acta Crystallogr. D66*, 213−221.
(32) Shaffer, P. L., Goehring, A., Shankaranarayanan, A., and Gouaux, E. (2009) Structure and mechanism of a Na^+-independent amino acid transporter. *Science 325*, 1010−1014.
(33) Becker, M., Bunikis, J., Lade, B. D., Dunn, J. J., Barbour, A. G., and Lawson, C. L. (2005) Structural investigation of *Borrelia burgdorferi* OspB, a bactericidal Fab target. *J. Biol. Chem. 280*, 17363−17370.
(34) Emsley, P., and Cowtan, K. (2004) Coot: Model-building tools for molecular graphics. *Acta Crystallogr. D60*, 2126−2132.
(35) Kaplan, A. P., Hood, L. E., Terry, W. D., and Metzger, H. (1971) Amino terminal sequences of human immunoglobulin heavy chains. *Immunochemistry 8*, 801−811.
(36) *Maestro*, version 9.1 (2010) Schrödinger, LLC, New York.
(37) Halgren, T. A., Murphy, R. B., Friesner, R. A., Beard, H. S., Frye, L. L., Pollard, W. T., and Banks, J. L. (2004) Glide: A new approach for rapid, accurate docking and scoring. 2. Enrichment factors in database screening. *J. Med. Chem. 47*, 1750−1759.
(38) Friesner, R. A., Murphy, R. B., Repasky, M. P., Frye, L. L., Greenwood, J. R., Halgren, T. A., Sanschagrin, P. C., and Mainz, D. T. (2006) Extra precision Glide: Docking and scoring incorporating a model of hydrophobic enclosure for protein-ligand complexes. *J. Med. Chem. 49*, 6177−6196.
(39) Friesner, R. A., Banks, J. L., Murphy, R. B., Halgren, T. A., Klicic, J. J., Mainz, D. T., Repasky, M. P., Knoll, E. H., Shelley, M., Perry, J. K., Shaw, D. E., Francis, P., and Shenkin, P. S. (2004) Glide: A new approach for rapid, accurate docking and scoring. 1. Method and assessment of docking accuracy. *J. Med. Chem. 47*, 1739−1749.
(40) *Glide*, version 5.6 (2010) Schrödinger, LLC, New York.
(41) *MacroModel*, version 9.8 (2010) Schrödinger, LLC, New York.
(42) Frank, M., Lutteke, T., and von der Lieth, C. W. (2007) GlycoMapsDB: A database of the accessible conformational space of glycosidic linkages. *Nucleic Acids Res. 35*, 287−290.
(43) Stanfield, R. L., Zemla, A., Wilson, I. A., and Rupp, B. (2006) Antibody elbow angles are influenced by their light chain class. *J. Mol. Biol. 357*, 1566−1574.
(44) Lee, M., Lloyd, P., Zhang, X., Schallhorn, J. M., Sugimoto, K., Leach, A. G., Sapiro, G., and Houk, K. N. (2006) Shapes of antibody binding sites: Qualitative and quantitative analyses based on a geomorphic classification scheme. *J. Org. Chem. 71*, 5082−5092.
(45) Kabat, E. A. (1966) The nature of an antigenic determinant. *J. Immunol. 97*, 1−11.
(46) Padlan, E. A., and Kabat, E. A. (1988) Model-building study of the combining sites of two antibodies to $\alpha(1\rightarrow6)$dextran. *Proc. Natl. Acad. Sci. U.S.A. 85*, 6885−6889.
(47) Agostino, M., Jene, C., Boyle, T., Ramsland, P. A., and Yuriev, E. (2009) Molecular docking of carbohydrate ligands to antibodies: Structural validation against crystal structures. *J. Chem. Inf. Model. 49*, 2749−2760.
(48) Bundle, D. R., Baumann, H., Brisson, J. R., Gagne, S. M., Zdanov, A., and Cygler, M. (1994) Solution structure of a trisaccharide-antibody complex: Comparison of NMR measurements with a crystal structure. *Biochemistry 33*, 5183−5192.
(49) Cygler, M., Rose, D. R., and Bundle, D. R. (1991) Recognition of a cell-surface oligosaccharide of pathogenic *Salmonella* by an antibody Fab fragment. *Science 253*, 442−445.
(50) Cygler, M., Wu, S., Zdanov, A., Bundle, D. R., and Rose, D. R. (1993) Recognition of a carbohydrate antigenic determinant of *Salmonella* by an antibody. *Biochem. Soc. Trans. 21*, 437−441.
(51) Zdanov, A., Li, Y., Bundle, D. R., Deng, S. J., MacKenzie, C. R., Narang, S. A., Young, N. M., and Cygler, M. (1994) Structure of a single-chain antibody variable domain (Fv) fragment complexed with a carbohydrate antigen at 1.7-Å resolution. *Proc. Natl. Acad. Sci. U.S.A. 91*, 6423−6427.
(52) Theillet, F. X., Saul, F. A., Vulliez-Le Normand, B., Hoos, S., Felici, F., Weintraub, A., Mulard, L. A., Phalipon, A., Delepierre, M., and Bentley, G. A. (2009) Structural mimicry of O-antigen by a peptide revealed in a complex with an antibody raised against *Shigella flexneri* serotype 2a. *J. Mol. Biol. 388*, 839−850.
(53) Vulliez-Le Normand, B., Saul, F. A., Phalipon, A., Belot, F., Guerreiro, C., Mulard, L. A., and Bentley, G. A. (2008) Structures of synthetic O-antigen fragments from serotype 2a *Shigella flexneri* in complex with a protective monoclonal antibody. *Proc. Natl. Acad. Sci. U.S.A. 105*, 9976−9981.
(54) Vyas, N. K., Vyas, M. N., Chervenak, M. C., Bundle, D. R., Pinto, B. M., and Quiocho, F. A. (2003) Structural basis of peptide-carbohydrate mimicry in an antibody-combining site. *Proc. Natl. Acad. Sci. U.S.A. 100*, 15023−15028.
(55) Vyas, N. K., Vyas, M. N., Chervenak, M. C., Johnson, M. A., Pinto, B. M., Bundle, D. R., and Quiocho, F. A. (2002) Molecular recognition of oligosaccharide epitopes by a monoclonal Fab specific for *Shigella flexneri* Y lipopolysaccharide: X-ray structures and thermodynamics. *Biochemistry 41*, 13575−13586.
(56) Bossart-Whitaker, P., Chang, C. Y., Novotny, J., Benjamin, D. C., and Sheriff, S. (1995) The crystal structure of the antibody N10-staphylococcal nuclease complex at 2.9 Å resolution. *J. Mol. Biol. 253*, 559−575.
(57) Eghiaian, F., Grosclaude, J., Lesceu, S., Debey, P., Doublet, B., Treguer, E., Rezaei, H., and Knossow, M. (2004) Insight into the PrPC → PrPSc conversion from the structures of antibody-bound ovine prion scrapie-susceptibility variants. *Proc. Natl. Acad. Sci. U.S.A. 101*, 10254−10259.
(58) Ding, W., Huang, X., Yang, X., Dunn, J. J., Luft, B. J., Koide, S., and Lawson, C. L. (2000) Structural identification of a key protective B-cell epitope in Lyme disease antigen OspA. *J. Mol. Biol. 302*, 1153−1164.
(59) McKern, N. M., Lawrence, M. C., Streltsov, V. A., Lou, M. Z., Adams, T. E., Lovrecz, G. O., Elleman, T. C., Richards, K. M., Bentley, J. D., Pilling, P. A., Hoyne, P. A., Cartledge, K. A., Pham, T. M., Lewis, J. L., Sankovich, S. E., Stoichevska, V., Da Silva, E., Robinson, C. P., Frenkel, M. J., Sparrow, L. G., Fernley, R. T., Epa, V. C., and Ward, C. W. (2006) Structure of the insulin receptor ectodomain reveals a folded-over conformation. *Nature 443*, 218−221.
(60) Braden, B. C., Goldbaum, F. A., Chen, B. X., Kirschner, A. N., Wilson, S. R., and Erlanger, B. F. (2000) X-ray crystal structure of an anti-Buckminsterfullerene antibody fab fragment: Biomolecular recognition of C(60). *Proc. Natl. Acad. Sci. U.S.A. 97*, 12193−12197.

(61) Rasmussen, S. G., Choi, H. J., Rosenbaum, D. M., Kobilka, T. S., Thian, F. S., Edwards, P. C., Burghammer, M., Ratnala, V. R., Sanishvili, R., Fischetti, R. F., Schertler, G. F., Weis, W. I., and Kobilka, B. K. (2007) Crystal structure of the human β2 adrenergic G-protein-coupled receptor. *Nature 450*, 383−387.

(62) Akagawa, M., Ito, S., Toyoda, K., Ishii, Y., Tatsuda, E., Shibata, T., Yamaguchi, S., Kawai, Y., Ishino, K., Kishi, Y., Adachi, T., Tsubata, T., Takasaki, Y., Hattori, N., Matsuda, T., and Uchida, K. (2006) Bispecific abs against modified protein and DNA with oxidized lipids. *Proc. Natl. Acad. Sci. U.S.A. 103*, 6160−6165.

(63) Al-Lazikani, B., Lesk, A. M., and Chothia, C. (1997) Standard conformations for the canonical structures of immunoglobulins. *J. Mol. Biol. 273*, 927−948.